UROP Report

Jonathan Ferguson Barry

September 7, 2018

CRSID: jfb52
College: St. John's

Nomenclature

Blade Angles

α_1	Absolute Rotor Inlet Angle	$^\circ$
α_2	Absolute Rotor Outlet Angle	$^\circ$
$\alpha_{1,rel}$	Relative Rotor Inlet Angle	$^\circ$
$\alpha_{2,rel}$	Relative Stator Inlet Angle	$^\circ$
χ_1^r	Rotor Inlet Metal Angle	$^\circ$
χ_2^r	Rotor Outlet Metal Angle	$^\circ$
χ_2^s	Stator Inlet Metal Angle	$^\circ$
χ_3^s	Stator Outlet Metal Angle	$^\circ$
δ	Deviation	$^\circ$
θ	Rotor Camber	$^\circ$
i_1	Rotor Inlet Incidence	$^\circ$
i_2	Stator Inlet Incidence	$^\circ$

Blade Geometry

c	Blade Chord	m
s	Blade Pitch	m
t	Blade Thickness	m
Z	Blade Number	m

Geometry

r_c	Casing Radius	m
r_h	Hub Radius	m
r_m	Mean-line Radius	m

Non-dimensional Properties

Λ	Reaction	
ϕ	Flow Coefficient	
ψ	Stage Loading Coefficient	

Other Symbols

$\dot{m}$	Mass Flow Rate	$Kgms^{-1}$
$\dot{Q}$	Volumetric Flow Rate	m^3s^{-1}
σ_y	Yield Stress	MPa
σ_{ts}	Tensile Strength	MPa
AR	Aspect Ratio	
F	Thrust	N
NR	Nozzle Ratio	
P	Power In	W

Subscripts

$()_0$	Intake Mouth
$()_1$	Rotor Inlet
$()_2$	Rotor Exit / Stator Inlet
$()_3$	Stator Outlet
$()_\infty$	Free-stream
$()_\theta$	Tangential
$()_c$	Casing
$()_h$	Hub
$()_m$	Mid-span
$()_r$	Rotor Blade
$()_s$	Stator Blade
$()_x$	Axial

1 Design Code

To assist with the fan design, a Matlab script was used to perform key calculations, treating the fan as a compressor stage. This section outlines the key assumptions made and the theory used to perform all the relevant calculations in the script.

1.1 Key Assumptions

The following assumptions were used throughout the analysis:

- Working fluid is air with international standard atmospheric pressure and density at sea level
- Axial velocity is constant throughout
- There is no swirl at inlet and outlet
  - Inlet and outlet flows are axial only
- The streamlines leaving the nozzle are straight and parallel in the axial direction
  - Implies that the exit flow must be at atmospheric pressure

1.2 Thrust and Power

1. Calculate variation in V_x, ϕ and ψ along blade span
   - Solve radial equilibrium equation for $\psi = \psi_m \left(\frac{r_m}{r}\right)^{n+1}$, using $n = 0.1$ as per previous design
   - Use ψ to obtain Δh_0 across rotor
   - Forward and backward Euler Methods gives variation in V_x across span
   - Use V_x to calculate ϕ across the span
2. Integrate across rotor span for total mass flow rate, $\dot{m}$ and stagnation enthalpy change, $\Delta h_{0,total}$
3. Obtain stagnation pressure rise across rotor using the assumed isentropic propulsor efficiency from previous design
4. Use continuity and Bernoulli to obtain remaining static pressures, stagnation pressures and absolute velocities
5. A control volume analysis using the SFME gives the thrust of the propulsor
6. The shaft power is found using the now known stagnation enthalpy change
   - An assumed motor efficiency of 90% was used to calculate the input electrical power

1.3 Flow angles and velocity triangles

All velocity triangle components were then calculated, this process was vectorised giving the parameters for various span-wise positions. In addition the reaction, Λ could then be calculated.

1.4 Blade Numbers

1. Calculate the pitch-to-chord ratio of both the rotor and stator blades using eqs. (1) and (2) respectively
    - Uses an assumed value for the diffusion factor, $DF = 0.45$ which is a typical value for a well designed blade row
    - This is a rearrangement of the incompressible case of Lieblein's equation for diffusion factor
2. Calculate the required number of rotor and stator blades using the blade pitch and circumference at the mid-span

$$\left(\frac{s}{c}\right)_r = \frac{2\left(DF - 1 + \frac{cos\alpha_{1,rel}}{cos\alpha_{2,rel}}\right)}{cos\alpha_{1,rel}\left(tan\alpha_{1,rel} - tan\alpha_{2,rel}\right)} \tag{1}$$

$$\left(\frac{s}{c}\right)_s = \frac{2\left(DF - 1 + \frac{cos\alpha_3}{cos\alpha_4}\right)}{cos\alpha_3\left(tan\alpha_3 - tan\alpha_4\right)} \tag{2}$$

1.5 Blade Metal Angles

The following method was used to calculate the required rotor and stator metal angles, both of which have initially been given an incidence of $-5°$. The final blade metal angles, as well as flow angles can be found in *table 3*.

1. Calculate rotor metal inlet angle
    - calculated using eq. (3) with known relative flow angle into the rotor and incidence
2. Calculate rotor metal outlet angle
    - Uses Carter's rule for fluid deviation across a compressor cascade to calculate the rotor metal exit angle
    - Carter's rule can be rearranged so that the metal angle is given by eq. (5)
    - The parameter, m can be found using eq. (4) which has been correlated for a compressor cascade
3. Calculate stator metal inlet angle
    - calculated using eq. (6) with known absolute flow angle into the rotor and incidence
4. Axial flow at outlet is desired to maximise thrust, therefore the stator exit is axial, $\chi_2^s = 0$

$$\chi_1^r = |\alpha_{1,rel}| - i_1 \tag{3}$$

$$m = 0.23\left(2\frac{a}{l}\right)^2 + \frac{|\alpha_{2,rel}|}{500} \tag{4}$$

$$\chi_2^r = \frac{|\alpha_{2,rel}| - \chi_1^r m\sqrt{\frac{s}{c}}}{1 - m\sqrt{\frac{s}{c}}} \tag{5}$$

$$\chi_2^s = |\alpha_2| - i_2 \tag{6}$$

2 Initial Design

2.1 Motor Selection

The motor was selected based on the calculated power requirement of $1846W$, which was calculated assuming a motor efficiency of 90%, as well as the design operating speed of $6000RPM$. Therefore, the Turnigy RotoMax 50cc Size Brushless Outrunner Motor was proposed for the initial design, the key parameters of the motor performance can be found in *Table 1.* This shows that at the operating speed the motor will be sufficiently below its rated power and therefore no active cooling is recommended.

Parameter	Rated Value	Operating Value	Units
$Voltage$	44	34.9	V
$Current$	120	52.9	A
$Power$	5300	1846	W

Table 1: A summary of the motor used in the initial design

2.2 Initial Design Summary

The design codes described previously were used to produce an initial fan design, a summary of the key operating point parameters can be found in *Table 2.* The design codes also included a script which, given the blade angles found in *Table 3*, produced .ibl files of the blade geometry. These .ibl files were then transfered to a CAD package and used to produce CAD models of the initial propulsor design. This design included an initial tip gap of 0.5% of the casing radius, r_c and the suitability of this gap was later tested using an FEA analysis.

Geometry			Operating Point		
Parameter	Value	Units	Parameter	Value	Units
r_h	0.055	m	ϕ_m	0.6	N/A
r_c	0.12	m	ψ_m	0.35	N/A
r_m	0.0875	m	Λ	0.825	N/A
AR_r	1.8	N/A	Ω	6000	RPM
AR_r	1.8	N/A	P	1846	W

Table 2: A summary of the initial ducted fan design

Angle	Hub	Mid	Tip	Angle	Hub	Mid	Tip
α_1	0	0	0	χ_1^r	57.8	64.0	67.2
$\alpha_{1,rel}$	-52.8	-59.0	-62.2	χ_2^r	20.4	36.9	41.4
α_2	26.5	30.3	40.6	χ_2^s	31.5	35.3	45.6
$\alpha_{2,rel}$	-28.7	-47.3	-55.0	χ_3^s	0	0	0
i_1	-5	-5	-5	δ	3.9	3.6	0.9
i_2	-5	-5	-5	θ	16.2	8.8	1.5

Table 3: A summary of the initial flow and blade angles

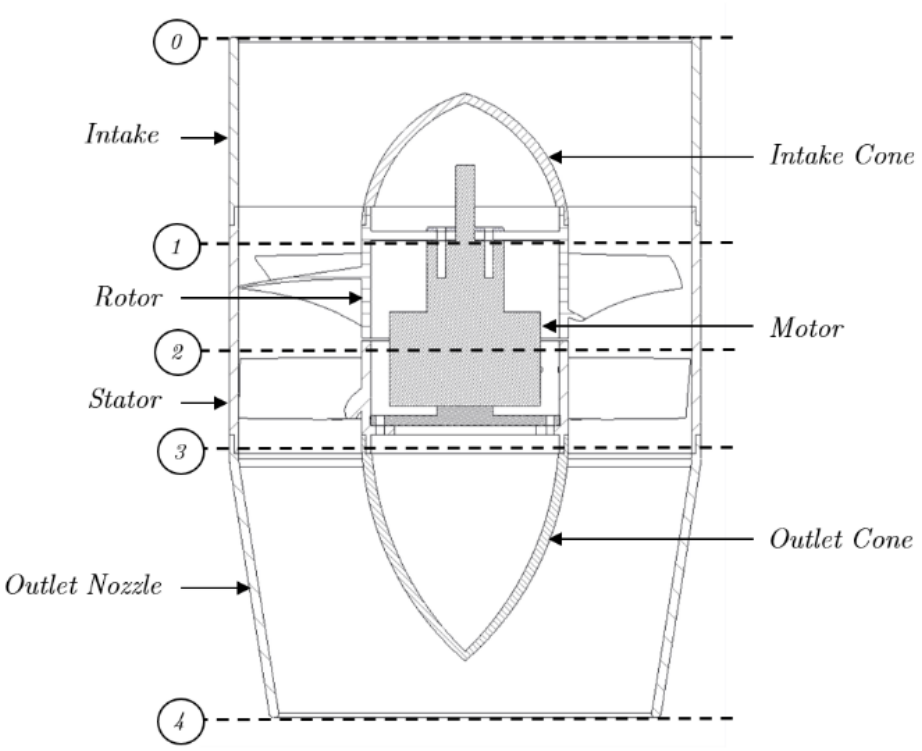

Figure 1: A cross-sectional diagram of the initial propulsor design

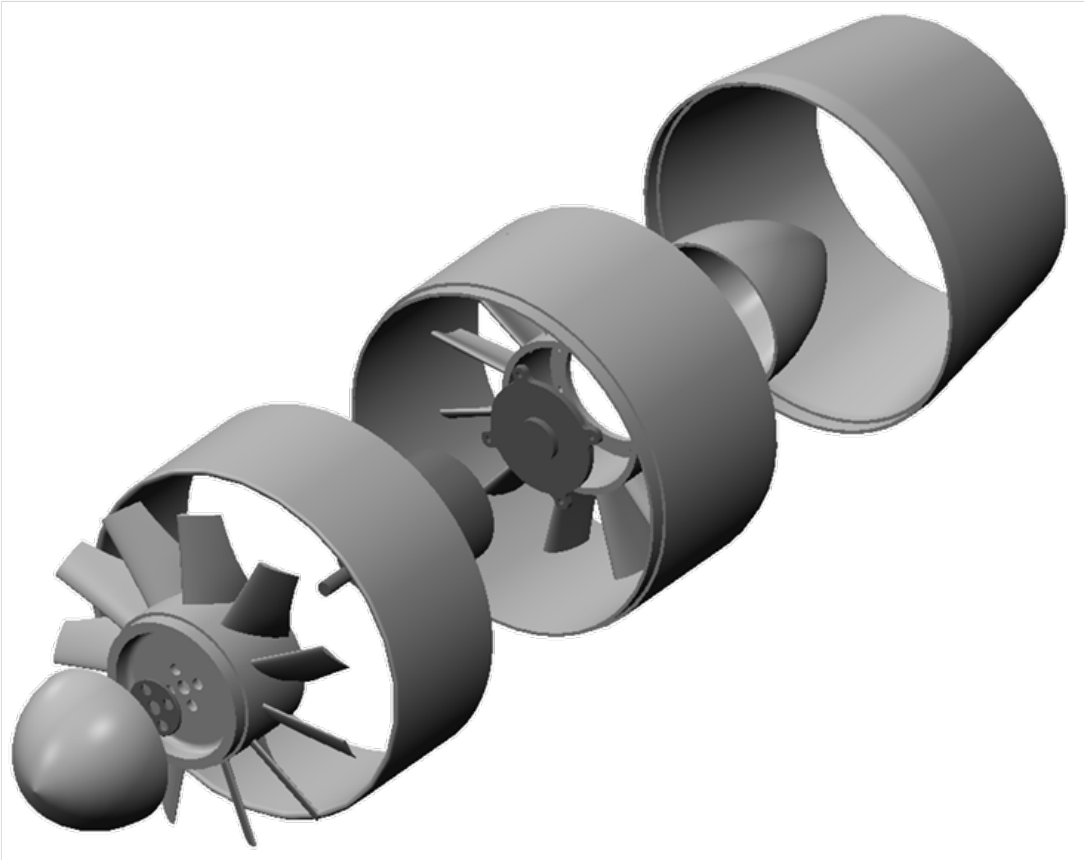

Figure 2: An exploded view of the initial propulsor design

3 Material Selection

Material selection for the rotor is crucial due to the large centrifugal stresses it experiences at the operating speed of $6000RPM$. It is desirable that components can be 3D printed in either the Whittle Lab or the Dyson Centre where possible, therefore polymers suitable for this were investigated, including PLA, ABS and Nylon. In addition, Al2014 Aluminium alloy was also investigated as an alternative material that could also be machined in the Whittle lab on a 5-axis CNC Milling machine.

3.1 FEA Results

The most important results for each material were whether the centrifugal stresses would cause the rotor to undergo plastic deformation or tensile failure. Therefore a CAD model was used to perform a Finite Element Analysis (FEA) at the operating speed. This simulation was carried out for each of the materials mentioned previously and the key material and test data can be found in *Table 4*, where:

- The maximum stress recorded is given by Von Mises
- The maximum displacement is the radial displacement at the blade tip

Material Properties			FEA Results	
Name	σ_y (MPa)	σ_{ts} (MPa)	Max. Stress (MPa)	Max. Displacement (mm)
PLA	63.5	58.5	9.8	0.330
ABS	29.6	36.9	8.2	0.392
Nylon	26.0	32.0	9.5	0.272
Al2014	29.6	36.9	19.8	0.035

Table 4: A summary of the mechanical properties and FEA results for the materials tested

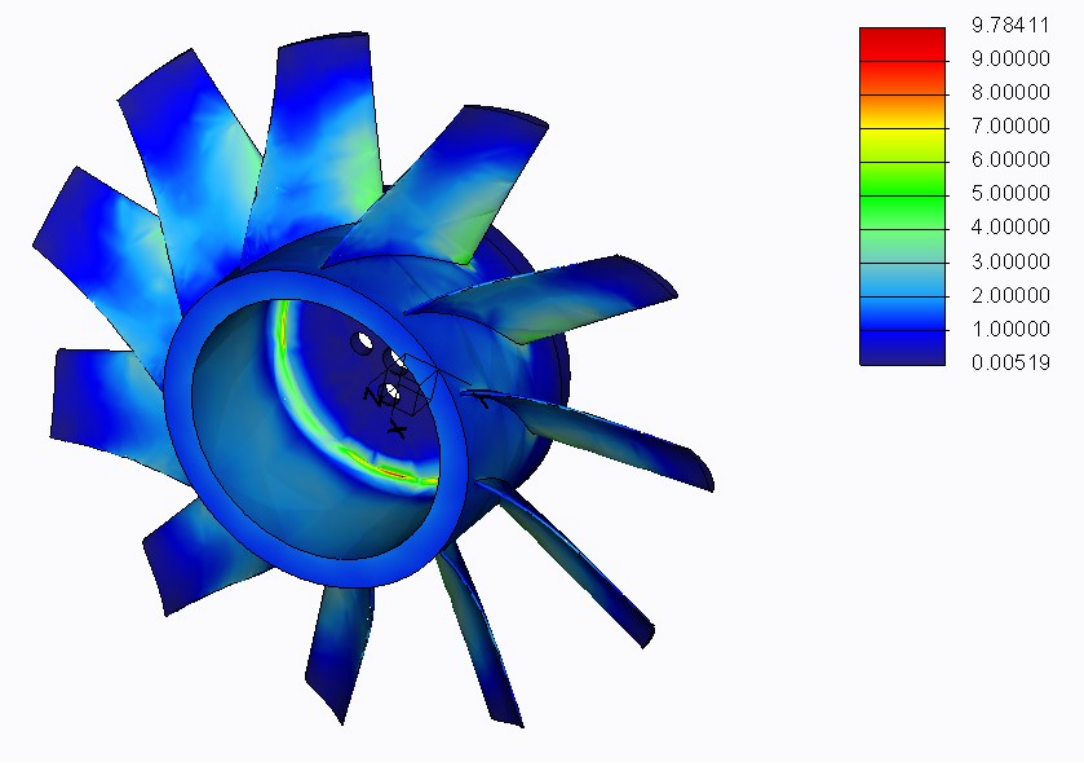

Figure 3: The FEA results for the rotor design, 3D printed from PLA (stresses shown in MPa)

3.2 Proposed Material and Tip Gap

Based on the FEA results for the proposed rotor design, PLA appears to be the most suitable material as it is suitable for 3D printing and will withstand the centrifugal forces at the operating speed. In addition, it gives a relatively low radial tip displacement due to elastic deflection of $0.33mm$. Therefore this material is proposed for the rotor, implemented with a tip gap of 0.7% of the casing radius, giving a gap of $0.84mm$ and a safety factor of 2.55.

4 Performance Characterisation

In order to characterise the performance of the ducted-fan design we require measurement of the flow field both upstream of the rotor and downstream of the stator, this will be done with 5-hole probes. Due to the rotation of the rotor we do not expect the flow field to vary in the circumferential direction upstream of the rotor, therefore a radial traverse only is suitable here. However, the flow field aft of the stator is expected to be stable with circumferential variation and therefore both a radial and circumferential traverse are required here

For the purposes of these initial tests, a baseline intake ans exit nozzle were designed to give the most favourable conditions possible for the fan. Therefore, a wide bell-mouth intake and a long converging exit nozzle were used.

4.1 Radial Traverse

The radial traverse used for the stator exit can be seen attached to the exit nozzle in fig. 4. The cross-sectional view in fig. 5 illustrates how control of the servo motor allows the radial probe position to be changed via the lead screw. Furthermore, the cross-sectional view in fig. 6 shows how the traverse frame is assembled from pieces machined from sheet aluminium.

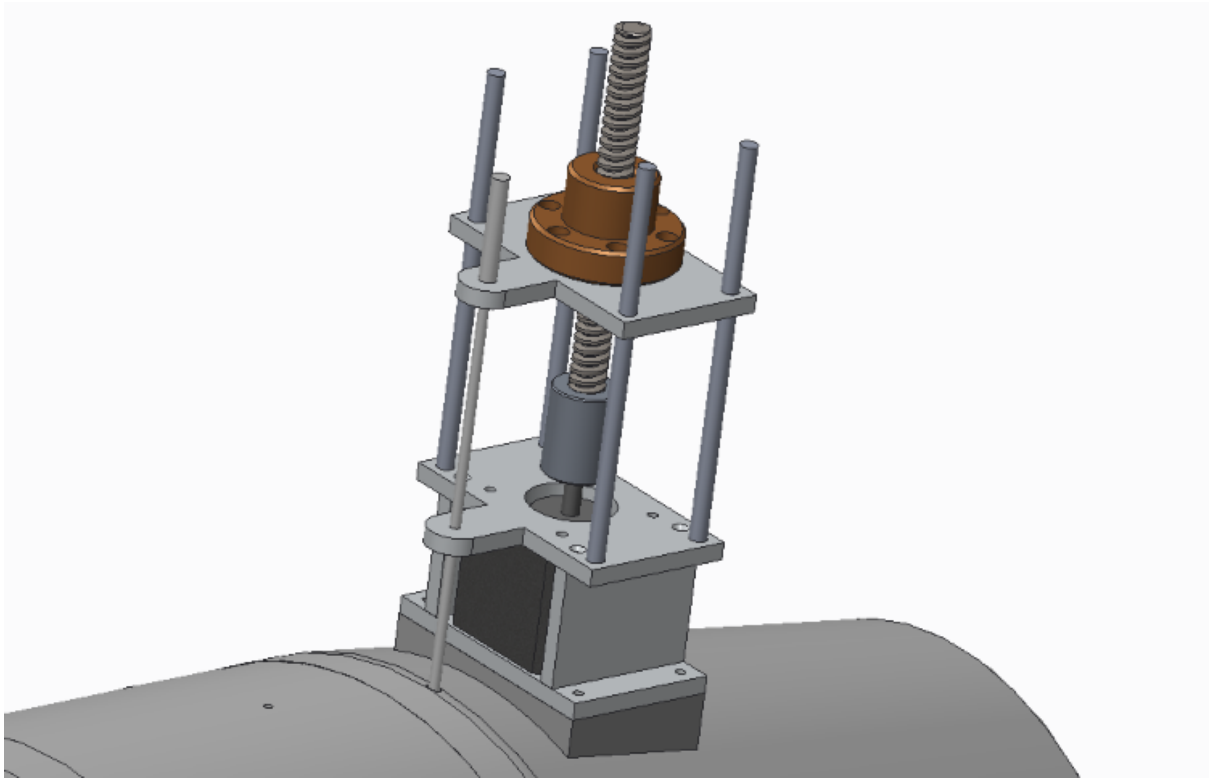

Figure 4: The radial traverse mounted on the exit nozzle

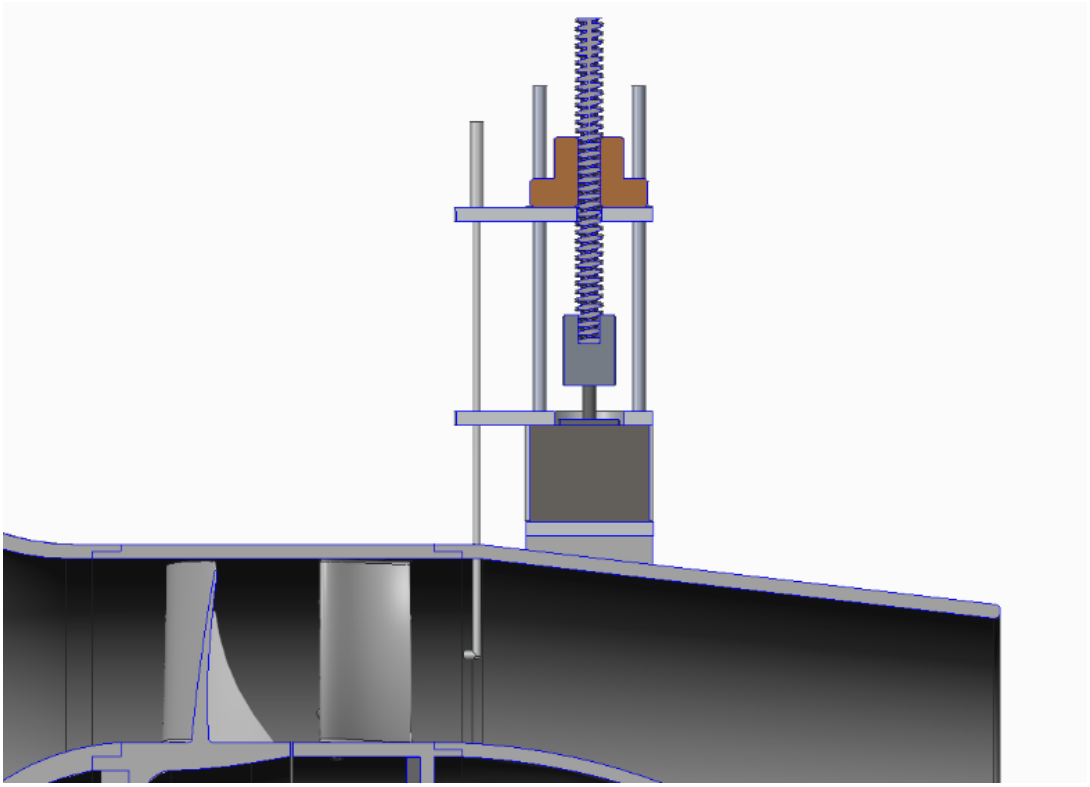

Figure 5: A cross-sectional view of the radial traverse mounted on the exit nozzle

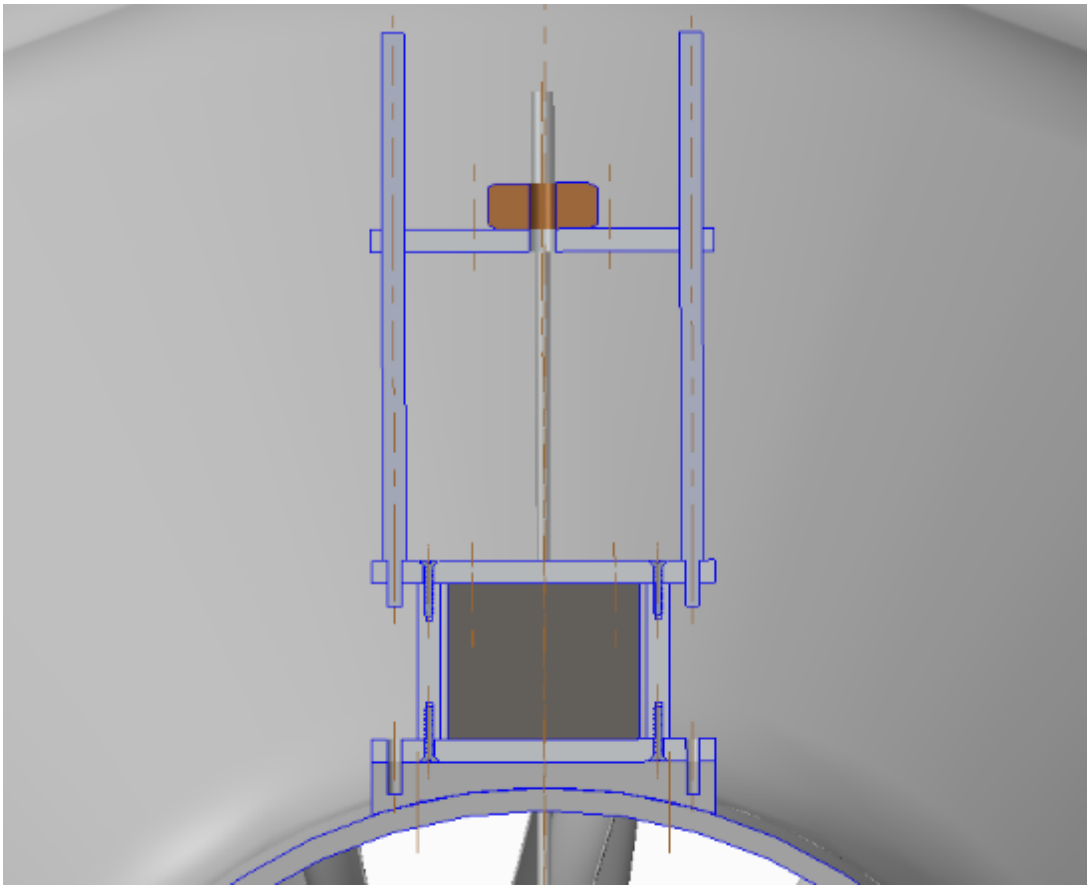

Figure 6: The radial traverse used to move a 5-hole probe radially for initial testing

4.2 Circumferential Traverse

To allow the probe to be moved circumferentially at the stator exit, it was decided to mount the exit nozzle on a slot and the entire nozzle to rotate. The nozzle was therefore split into sections, allowing it to be secured onto the slot and the probe to be inserted. An additional servo motor will be mounted on the stator section of the fan as shown in figs. 7 and 8, which is used to rotate the exit nozzle across a 90° span using the gear mechanism.

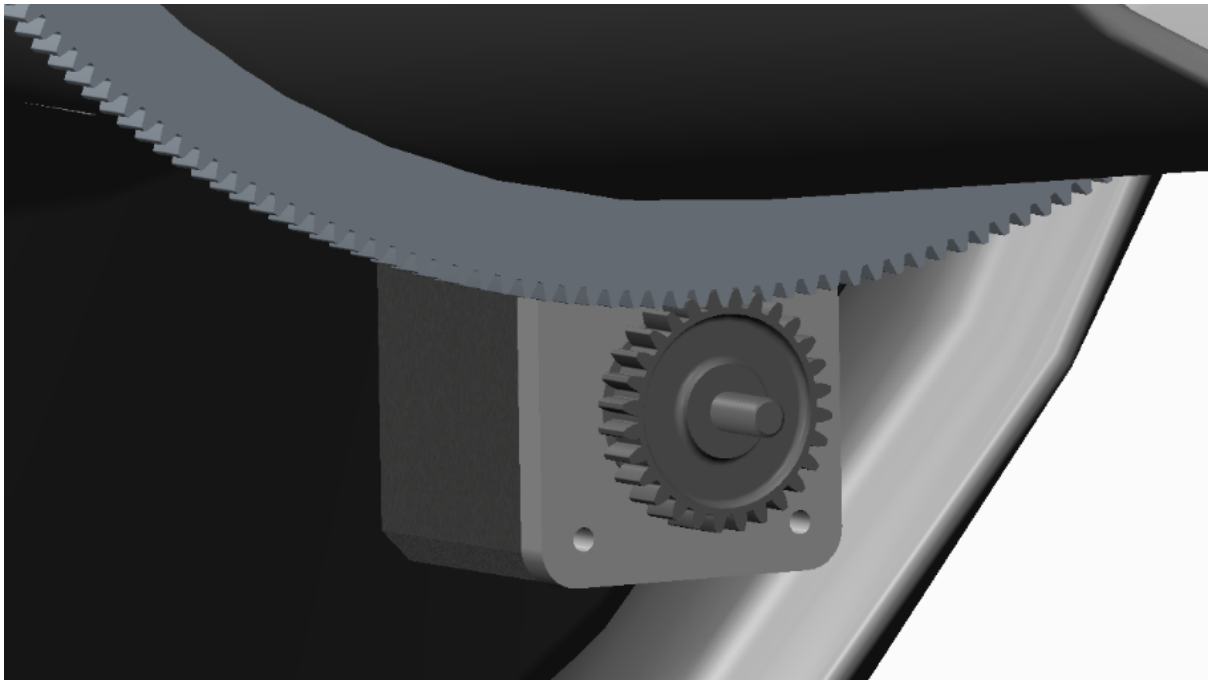

Figure 7: The circumferential traverse used for rotating the exit nozzle, moving the 5-hole probe circumstantially

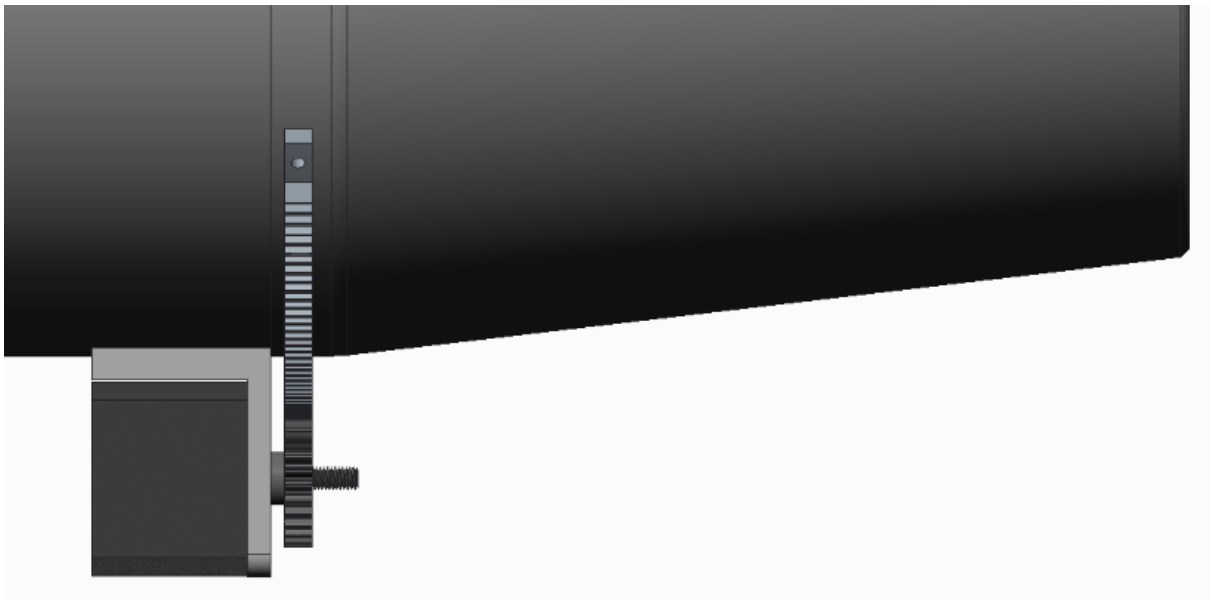

Figure 8: The gear mechanism used for rotating the exit nozzle

5 Final Design

Incremental improvements were made until the final design was reached, this section will describe the key improvements made to the rotor and stator section. The rotor and stator sections will both be 3D printed in PLA, this will be done by Selective Laser Sintering (SLS) by Protolabs as it offers a high-quality finish and is suitable for thin sections.

5.1 Rotor Design

Two main improvement were made to the rotor design:

- A taper was added to the inside wall
  - This reduces the radial displacement at the operating speed by reducing the mass and centrifugal stresses
- Compartments were added to the top surface
  - This allows material such as plasticine to be added to balance the rotor if required

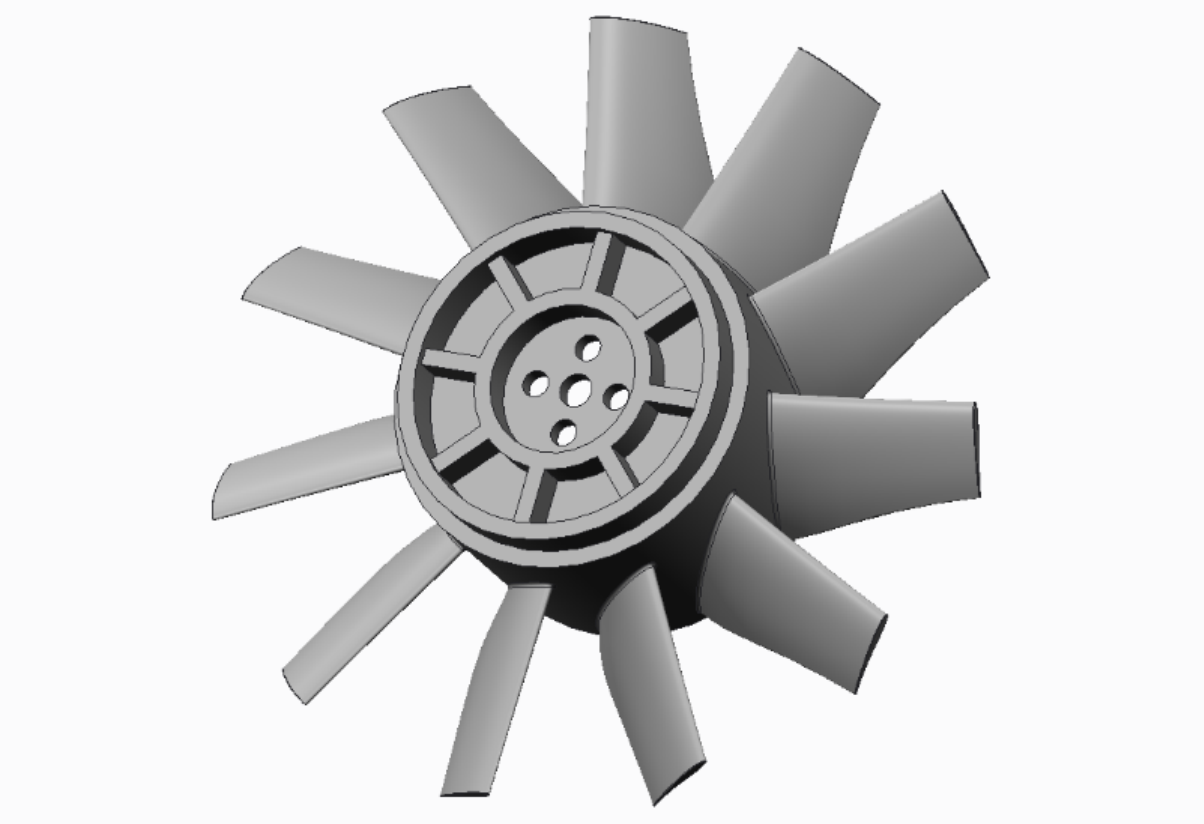

Figure 9: The final rotor design to be 3D printed

5.2 Stator Section Design

As the central component of the design, a number of changes were made to the stator section which included:

- Holes on the surface for mounting traverse brackets and the load cells
  - These holes will be fitted with helicoil inserts to allow the brackets to be screwed in place
- Holes for the motor cables were added to the inside of selected stator blades
  - Each of the three motor wires will split into two along the stator blades to distribute the large currents between thinner gauge wires
- Grooves to hold the intake and exit nozzle in place were added
- The stator blades were given a parabolic stacking profile

The final stator design can be seen in fig. 10.

Figure 10: The final stator section design to be 3D printed

6 Appendices

6.1 Radial Equilibrium Theory

The variation of the swirl distribution at the rotor exit is given by eq. (7).

$$V_{\theta 2} r^n = k \tag{7}$$

Starting from the definition of the stage loading coefficient and assuming there is no swirl at the rotor inlet, $V_{\theta 1} = 0$ we can rearrange this to obtain eq. (8).

$$\begin{aligned} \psi &= \frac{\Delta\big(UV_\theta\big)}{U^2} \\ &= \frac{UV_{\theta 2} - UV_{\theta 1}}{U^2} \\ &= \frac{V_{\theta 2}}{U} \\ \Rightarrow V_{\theta 2} &= \psi U \end{aligned} \tag{8}$$

In order to obtain a value for the constant, k in eq. (7) we first need to evaluate $V_{\theta 2}$ at the mid-span. Therefore substituting eq. (8) for $V_{\theta 2,m}$ into eq. (7) we obtain a value for k given by eq. (9).

$$k = \psi_m U_m r_m^n \tag{9}$$

This value of k is then substituted back into eq. (7) and rearranged for ψ which is a function of the radial position, r. Further simplification is made using the substitution for the blade speed, $U = \omega r$ giving eq. (10).

$$\begin{aligned} \psi\big(r\big)U\big(r\big)r^n &= \psi_m U_m r_m^n \\ \psi\big(r\big) &= \psi_m \left(\frac{U_m}{U\big(r\big)}\right)\left(\frac{r_m}{r}\right)^n \\ &= \psi_m \left(\frac{\omega r_m}{\omega r}\right)\left(\frac{r_m}{r}\right)^n \\ &= \psi_m \left(\frac{r_m}{r}\right)^{n+1} \end{aligned} \tag{10}$$